Journal of Systems Engineering and Electronics
Vol. 34, No. 6, December 2023, pp.1526 – 1536

Ambiguity function analysis and side peaks suppression of Link16 signal based passive radar

BAI Luyang, WANG Jun*, and CHEN Xiaoling

National Key Laboratory of Radar Signal Processing, Xidian University, Xi'an 710071, China

Abstract: Link16 data link is the communication standard of the joint tactical information distribution system (JTIDS) used by the U.S. military and North Atlantic Treaty Organization, which is applied as the opportunistic illuminator for passive radar in this paper. The time-domain expression of the Link16 signal is established, and its ambiguity function expression is derived. The time-delay dimension and Doppler dimension side peaks of which lead to the appearance of the false target during target detection. To solve the problem, the time-delay dimension and Doppler dimension side peaks suppression methods are proposed. For the problem that the conventional mismatched filter (MMF) cannot suppress the time-delay dimension side peaks, a neighborhood MMF (NMMF) is proposed. Experimental results demonstrate the effectiveness of the proposed methods.

Keywords: passive radar, ambiguity function, Link16, mismatched filter (MMF).

DOI: 10.23919/JSEE.2023.000152

1. Introduction

Passive radar is a bistatic/multistatic radar with separate transmitters and receivers, which detects passively by receiving the signal of the opportunistic illuminators reflected by the target. It has the advantages of strong concealment, low cost, and no electromagnetic pollution. Passive radar based on frequency modulation (FM) radio [1−5], digital radio [6−8], analog television (ATV) [9−11], digital television [12−18], mobile communication [19−23], and other civil illuminators has been widely studied in recent years. However, in the battlefield environment such as ocean and desert, which is far away from densely populated areas, the passive radar is facing the problem of lacking civilian illuminators, so it cannot be used in these battlefield environments. In modern war, to realize information exchange and environment perception functions such as communication and detection, there are a large number of military illuminators on the battlefield. Therefore, the study of passive radar based on military illuminators has a great applicable value.

Military illuminators generally include radar, tactical data link (TDL), tactical air navigation system (TACAN), and others. TDL, also known as Link in North Atlantic Treaty Organization (NATO), is used to transmit machine-readable tactical digital information as a standard communication link [24]. Link16 data link is the communication standard of the joint tactical information distribution system (JTIDS) used by the U.S. military and NATO, which is applied to the communication, navigation, and identification between aircraft, warship, and other weapon platforms. Meanwhile, Link16 is one of the most widely used TDL in the world, which makes it possible to use Link16 signal as the illuminators of passive radar in battlefield environment. However, the current research on Link16 data link is only limited to the field of communication, and there is no research on Link16 signal based passive radar.

Unlike active radar transmitting a designed waveform, passive radar uses non-cooperative opportunistic illuminators to detect targets. When the ambiguity function of the signal transmitted by opportunistic illuminators is not ideal, that is, the ambiguity function is not near thumbtack, these ambiguity ranges and Doppler side peaks will be detected as targets and degrade the target detection performance. Therefore, the side peaks of the ambiguity function must be suppressed before target detection. Side peak suppression methods in existing studies can be divided into two categories [25]. The first category suppresses the side peaks by removing or preprocessing the guard interval (GI) and cyclic prefix (CP) in the signal frame. This method needs to know the frame structure of the signal and is mostly used for digitally modulated signals, such as Wi-Fi [26−29] and digital television

Manuscript received July 30, 2021.
*Corresponding author.
This work was supported by the National Natural Science Foundation of China (61401526).

[13,30−32]. The second method is based on mismatched filter (MMF). MMF is relative to matched filter (MF), which was first used to improve the phase-coded radar waveforms' side lobe structure [33]. In [11], the author applied the MMF method to suppress the time-delay dimension side peaks of ATV-based passive radar for the first time. MMF achieves the purpose of side peak suppression by establishing a cost function and solving the optimal MMF factor and then performing mismatch processing on the reference signal. This method does not need to know the structure of the signal accurately, and only needs to know the position of the side peaks on the range-Doppler surface, and it is mainly applied to analog modulated signals. At present, there are also many studies on improving the cost function to obtain better side peaks suppression performance [15,34−36].

In this paper, Link16 signal is used as the illuminator of opportunity for passive radar, which is modeled mathematically and constructed time domain expression. Then, according to its definition, the ambiguity function of Link16 signal is deduced and the correctness is verified by simulation results. Subsequently, a neighborhood MMF (NMMF) algorithm is proposed to suppress the time-delay dimension side peaks, and this paper proposes a method of removing Doppler dimension side peaks.

The structure of this paper is organized as follows. In Section 2, the signal structure of Link16 is introduced and its time domain expression is established. In Section 3, the ambiguity function of Link16 signal is derived, and the cause of time-delay dimension and Doppler dimension side peaks is analyzed. In Section 4, the method of suppressing the side peaks is proposed. Finally, Section 5 presents the conclusions.

2. Structure of Link16 signal

Link16 data link is composed of J series message standard, JTIDS waveform, and time division multiple access (TDMA) protocol. In detail, the J series message is defined by the U.S. standard MIL-STD-6016 or NATO standard STANAG5516 and STANAG5616, which is the baseband information transmitted by the Link16 data link. JTIDS waveform is the transmitting signal which is suitable for transmission and strong anti-interference converted by JTIDS unit (JU) according to J series messages. TDMA protocol is used to control user access.

Take the single network structure as an example, the time slot division of Link16 is shown in Fig. 1. The TDMA protocol divides a 24-hour day into 112.5 epochs, and each epoch is 12.8 min in duration; each epoch is divided into 64 frames, and each frame is 12 s in duration. Each frame is further divided into 1536 time slots, each one of which is 7.8125 ms in duration. The time slot is the basic unit of access to the Link16 network.

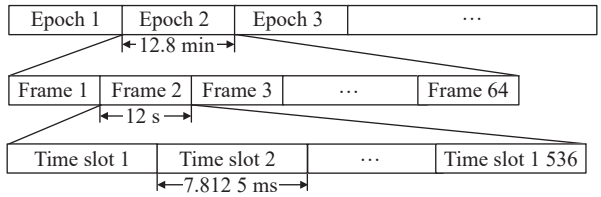

Fig. 1 Diagram of Link16 time slot division

In a time slot, according to different data pulse formats, it can be divided into four packaging structures: standard double pulse (STDP), packed-2 single pulse (P2SP), packed-2 double pulse (P2DP), and packed-4 single pulse (P4SP). In order to ensure the strongest anti-interference performance, Link16 system usually uses STDP package, and its structure is shown in Fig. 2. Therefore, this paper mainly studies the Link16 signal using STDP packaging structure.

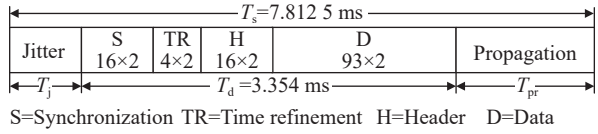

Fig. 2 STDP package structure

As shown in Fig. 3, after receiving the J series messages generated by the Link16 unit, JU uses cyclic redundancy check (CRC) codes, reed-solomon (R-S) codes, interweave, cyclic code shift keying (CCSK) codes, codeword encryption, minimum shift keying (MSK) modulation, and frequency hopping, adding synchronous symbol and header to generate JTIDS waveform, with strong anti-interference capacity. Then package the waveform according to STDP package structure to generate the transmission signal.

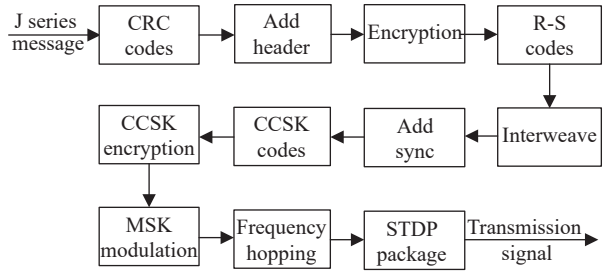

Fig. 3 Transmission signal generation process

It should be noted that CCSK is applied to the 5-bit interleaved symbols of the R-S codewords. Each 5-bit symbol is represented by a 32-bit sequence. The bits of this sequence are called chips to avoid confusion. These 32-chip sequences are derived by shifting an arbitrary

starting sequence number left one place each time, and each 5-bit interleaved symbol points to a specific chipping sequence. Since the 5-bit symbol's binary value can vary from 0 to 31, there are 32 unique chipping sequences S_0 to S_{31}.

Then, the encrypted CCSK codeword is modulated by MSK with a bit rate of R_b=5 Mb/s to obtain a single or double pulse symbol package as shown in Fig. 4, and the width of each MSK symbol is T_B=0.2 μs. Therefore, the length of 32 MSK symbols is 32 T_B = 6.4 μs. In Fig. 4, T_p is the pulse repetition period, and T_{pd} is the pulse width.

MSK modulation is a special frequency shift keying (FSK) modulation. Compared with 2FSK signal, MSK signal has the advantages of continuous phase, minimum bandwidth, constant envelope, and strictly orthogonal. The modulation diagram is shown in Fig. 5, where a_k is the symbol to be encoded, b_k is the symbol after differential encoding, p_k and q_k are the symbols after serial to parallel conversion, and f_c is the carrier frequency.

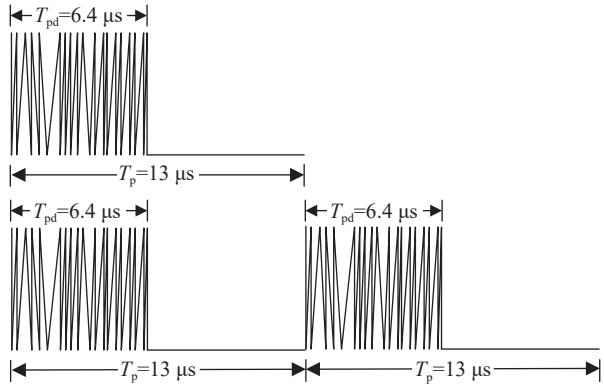

Fig. 4 Diagram of double and single pulse

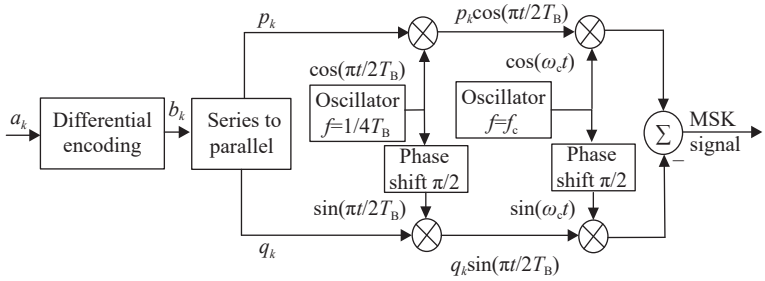

Fig. 5 Principle diagram of MSK quadrature modulation

Using orthogonal representation, the signal of the kth (k = 0,1,⋯,31) symbol modulated by MSK can be expressed as

$$s_k(t) = p_k \cos\frac{\pi t}{2T_B}\cos(\omega_c t) - q_k \sin\frac{\pi t}{2T_B}\sin\omega_c t,\ \ kT_B \leqslant t \leqslant (k+1)T_B \tag{1}$$

where $p_k = \pm 1$ and $q_k = \pm 1$ are serial to parallel converted symbols; ω_c is the angular frequency of carrier.

The baseband complex envelope of the ith pulse after MSK modulation is

$$m_i(t) = \sum_{k=0}^{31}\left(p_k \cos\frac{\pi t}{2T_B} - jq_k \sin\frac{\pi t}{2T_B}\right),\ \ kT_B \leqslant t \leqslant (k+1)T_B \tag{2}$$

And the signal of the valid portion in a time slot of the STDP package (remove jitter and propagation) can be expressed as

$$s_s(t) = \begin{cases} \sum_{i=0}^{257} m_i(t - iT_p)\mathrm{e}^{\mathrm{j}2\pi(f_c+\Delta f_i)(t-iT_p)}, \\ \qquad iT_p \leqslant t \leqslant iT_p + T_{pd} \\ 0, \ \text{otherwise} \end{cases} \tag{3}$$

where T_p = 13 μs; T_{pd} = 6.4 μs; Δf_i is the carrier frequency offset of the ith pulse compared to the first pulse. It needs to be clear that the pulses in the STDP package structure appear in pairs, that is, the same group of 32 MSK symbols are transmitted with two pulses with different carrier frequencies. Thus, there is $m_{2i-1} = m_{2i}$ (i = 0,1,⋯,128).

Considering the portion of jitter and propagation, the Link16 signal with N time slots can be expressed as

$$s(t) = \begin{cases} \sum_{n=0}^{N-1} s_{s,n}(t - nT_s - T_j), \\ \qquad nT_s + T_j \leqslant t \leqslant nT_s + T_j + T_d \\ 0, \ \text{otherwise} \end{cases} \tag{4}$$

where T_s, T_j, and T_d are the length of time slot, the length of jitter and the length of valid portion, and $s_{s,n}$ is the signal transmitted in the nth time slot. Set T_{pr} as the length of propagation, and the STDP package structure specifies that T_s = 7.8125 ms, T_d = 3.354 ms, and T_j + T_{pr} = 4.4585 ms. In order to facilitate analysis without losing generality, this paper sets T_j = 2 ms and T_{pr} = 2.4585 ms.

Fig. 6 and Fig. 7 respectively show the time waveform and spectrum of the Link16 signal with 16 time slots which lasts for 0.125 s.

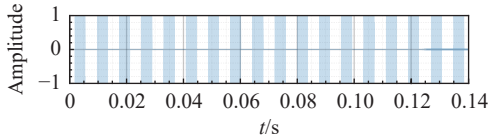

(a) Time waveforms of 16 time slots

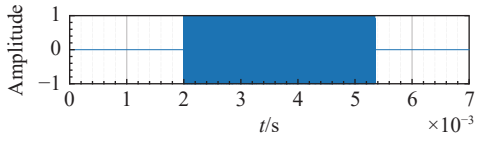

(b) Time waveforms of a single time slot

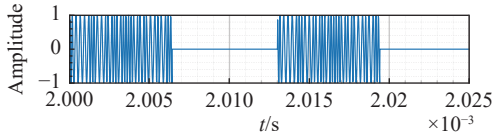

(c) Time waveforms of double pulses

Fig. 6 Time waveform of Link16 signal

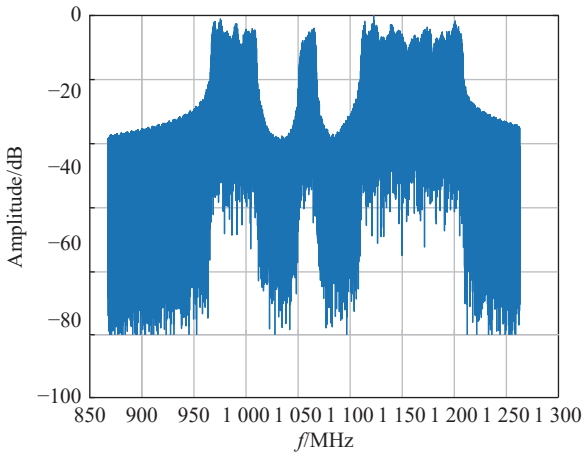

(a) Spectrum of RF signal

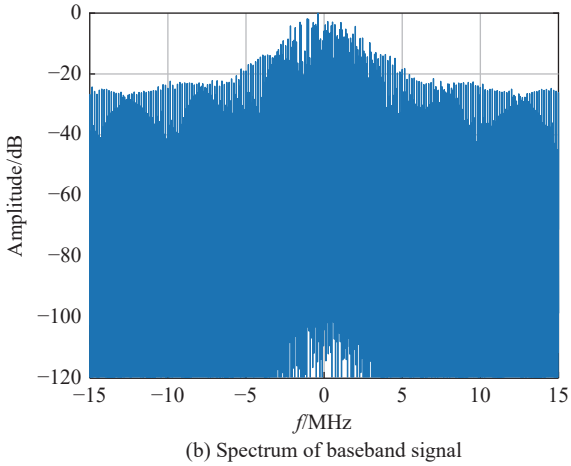

(b) Spectrum of baseband signal

Fig. 7 Spectrum of Link16 signal

Fig. 6, from top to bottom, respectively shows the time waveforms of 16 time slots, a single time slot and the double pulses. And the variable carrier frequency with no phase discontinuities can be observed, which is the basic feature of MSK modulation.

Fig. 7(a) is the spectrum of Link16 RF signal, which shows it works in frequency hopping between 960 MHz to 1 215 MHz, and Fig. 7(b) is the spectrum of the Link16 baseband signal which down-converts the RF signal according to hopping patterns. It can be seen that multiple discrete spectral lines are attached to the MSK signal power spectrum [37], which is caused by the truncation of the MSK signal by multiple pulses.

3. Ambiguity function analysis

The ambiguity function of the radar signal [38] is defined as

$$\chi(\tau, f_{\mathrm{d}}) = \int_{-\infty}^{+\infty} u(t)\, u^{*}(t-\tau)\, \mathrm{e}^{\mathrm{j}2\pi f_{\mathrm{d}} t}\, \mathrm{d}t \tag{5}$$

where τ is the time delay; f_{d} is the Doppler shift; $u(t)$ is the complex envelope of Link16 signal, which down-converts the RF signal according to hopping patterns; $(\cdot)^{*}$ represents complex conjugate operation. Fig. 8 shows the ambiguity function of the Link16 signal with 16 time slots generated by the simulation in Section 1, with 0 ms $\leqslant \tau \leqslant$ 0.2 ms and −2 000 Hz $\leqslant f_{\mathrm{d}} \leqslant$ 2 000 Hz. It can be seen from Fig. 8 that the ambiguity function of Link16 signal is composed of a main peak and a lot of side peaks which almost cover the whole delay-Doppler plane. In order to facilitate the analysis, the side peaks are divided into time-delay dimension side peaks and Doppler dimension side peaks, that is, one of the variables τ or f_{d} in $\chi(\tau, f_{\mathrm{d}})$ is taken as a fixed value, and the other is taken as a variable for analysis. When f_{d} is fixed, it is the time-delay dimension of the ambiguity function. Fig. 8(b) shows the zero Doppler cut $\chi(\tau, 0)$ when $f_{\mathrm{d}} = 0$ Hz. When τ is fixed, it is the Doppler dimension of the ambiguity function. Fig. 8(c) shows the zero delay cut $\chi(0, f_{\mathrm{d}})$ when $\tau = 0$.

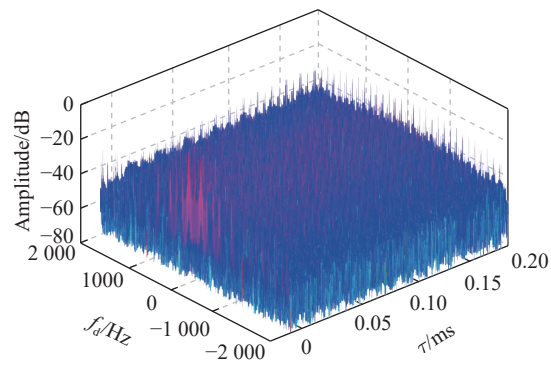

(a) Ambiguity function

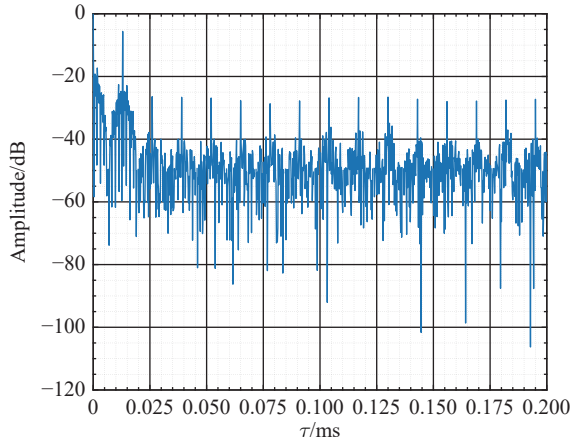

(b) Zero Doppler cut of ambiguity function

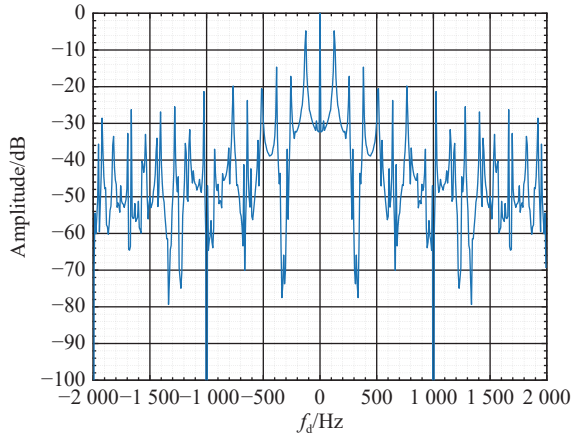

(c) Zero range cut of ambiguity func time

Fig. 8 Ambiguity function of Link16 signal

To analyze the ambiguity function of Link16 signal, combining (4) and (5), we can get

$$\chi(\tau,f_{\mathrm{d}})=\int_{-\infty}^{+\infty}\left(\sum_{n=0}^{N-1}s_{\mathrm{s},n}(t-nT_{\mathrm{s}}-T_{\mathrm{j}})\right)\cdot\left(\sum_{m=0}^{N-1}s^{*}{}_{\mathrm{s},m}(t-mT_{\mathrm{s}}-T_{\mathrm{j}}-\tau)\right)\mathrm{e}^{\mathrm{j}2\pi f_{\mathrm{d}}t}\mathrm{d}t=\sum_{n=0}^{N-1}\sum_{m=0}^{N-1}\int_{-\infty}^{+\infty}s_{\mathrm{s},n}(t-nT_{\mathrm{s}}-T_{\mathrm{j}})\cdot s^{*}{}_{\mathrm{s},m}(t-mT_{s}-T_{j}-\tau)\mathrm{e}^{\mathrm{j}2\pi f_{\mathrm{d}}t}\mathrm{d}t. \tag{6}$$

Let $t-nT_{\mathrm{s}}-T_{\mathrm{j}}=t_1$, then (6) can be written as

$$\chi(\tau,f_{\mathrm{d}})=\sum_{n=0}^{N-1}\sum_{m=0}^{N-1}\int_{-\infty}^{+\infty}s_{\mathrm{s},n}(t_1)\cdot s^{*}{}_{\mathrm{s},m}(t_1-[\tau-(n-m)T_{\mathrm{s}}])\mathrm{e}^{\mathrm{j}2\pi f_{\mathrm{d}}(nT_{\mathrm{s}}+T_{\mathrm{j}}+t_1)}\mathrm{d}t_1=\mathrm{e}^{\mathrm{j}2\pi f_{\mathrm{d}}T_{\mathrm{j}}}\sum_{n=0}^{N-1}\mathrm{e}^{\mathrm{j}2\pi f_{\mathrm{d}}nT_{\mathrm{s}}}\sum_{m=0}^{N-1}\chi_{\mathrm{s},nm}(\tau-(n-m)T_{\mathrm{s}},f_{\mathrm{d}}) \tag{7}$$

where the integral term represents the cross-ambiguity function of the nth time slot and the mth time slot, expressed by $\chi_{\mathrm{s},nm}$.

Let $n-m=k$ in (7), and use the double summation formula [39] as follows:

$$\sum_{n=0}^{N-1}\sum_{m=0}^{N-1}f(n,m)=\sum_{k=-(N-1)}^{0}\sum_{n=0}^{N-1-|k|}f(n,n-k)+\sum_{k=1}^{N-1}\sum_{m=0}^{N-1-|k|}f(m+k,m) \tag{8}$$

then (7) can be rewritten as

$$\chi(\tau,f_{\mathrm{d}})=\mathrm{e}^{\mathrm{j}2\pi f_{\mathrm{d}}T_{\mathrm{j}}}\left[\sum_{k=-(N-1)}^{0}\sum_{n=0}^{N-1-|k|}\left(\mathrm{e}^{\mathrm{j}2\pi f_{\mathrm{d}}nT_{\mathrm{s}}}\chi_{\mathrm{s},k}(\tau-kT_{\mathrm{s}},f_{\mathrm{d}})\right)+\sum_{k=1}^{N-1}\sum_{m=0}^{N-1-|k|}\left(\mathrm{e}^{\mathrm{j}2\pi f_{\mathrm{d}}(m+k)T_{\mathrm{s}}}\chi_{\mathrm{s},k}(\tau-kT_{\mathrm{s}},f_{\mathrm{d}})\right)\right]=\mathrm{e}^{\mathrm{j}2\pi f_{\mathrm{d}}T_{\mathrm{j}}}\left[\sum_{k=-(N-1)}^{0}\chi_{\mathrm{s},k}(\tau-kT_{s},f_{d})\sum_{n=0}^{N-1-|k|}\mathrm{e}^{\mathrm{j}2\pi f_{\mathrm{d}}nT_{\mathrm{s}}}+\sum_{k=1}^{N-1}\mathrm{e}^{\mathrm{j}2\pi f_{\mathrm{d}}kT_{\mathrm{s}}}\chi_{\mathrm{s},k}(\tau-kT_{\mathrm{s}},f_{\mathrm{d}})\sum_{m=0}^{N-1-|k|}\mathrm{e}^{\mathrm{j}2\pi f_{\mathrm{d}}mT_{\mathrm{s}}}\right]. \tag{9}$$

Perform the following summation of series:

$$\sum_{n=0}^{N-1-|k|}\mathrm{e}^{\mathrm{j}2\pi f_{\mathrm{d}}nT_{\mathrm{s}}}=\sum_{n=0}^{N-1-|k|}\left(\mathrm{e}^{\mathrm{j}2\pi f_{\mathrm{d}}T_{\mathrm{s}}}\right)^{n}=\frac{1-\left(\mathrm{e}^{\mathrm{j}2\pi f_{\mathrm{d}}T_{\mathrm{s}}}\right)^{N-|k|}}{1-\mathrm{e}^{\mathrm{j}2\pi f_{\mathrm{d}}T_{\mathrm{s}}}}=\frac{\left(\mathrm{e}^{\mathrm{j}2\pi f_{\mathrm{d}}T_{\mathrm{s}}}\right)^{\frac{N-|k|}{2}}}{\left(\mathrm{e}^{\mathrm{j}2\pi f_{\mathrm{d}}T_{\mathrm{s}}}\right)^{\frac{1}{2}}}\cdot\frac{\left(\mathrm{e}^{\mathrm{j}2\pi f_{\mathrm{d}}T_{\mathrm{s}}}\right)^{-\frac{N-|k|}{2}}-\left(\mathrm{e}^{\mathrm{j}2\pi f_{\mathrm{d}}T_{\mathrm{s}}}\right)^{\frac{N-|k|}{2}}}{\left(\mathrm{e}^{\mathrm{j}2\pi f_{\mathrm{d}}T_{\mathrm{s}}}\right)^{-\frac{1}{2}}-\left(\mathrm{e}^{\mathrm{j}2\pi f_{\mathrm{d}}T_{\mathrm{s}}}\right)^{\frac{1}{2}}}=\mathrm{e}^{\mathrm{j}\pi f_{\mathrm{d}}(N-1-|k|)T_{\mathrm{s}}}\frac{\sin\left[\pi f_{\mathrm{d}}(N-|k|)T_{\mathrm{s}}\right]}{\sin(\pi f_{\mathrm{d}}T_{\mathrm{s}})}. \tag{10}$$

Then substitute the sum result in (10) into (9), we get

$$\chi(\tau,f_{\mathrm{d}})=\mathrm{e}^{\mathrm{j}2\pi f_{\mathrm{d}}T_{\mathrm{j}}}\sum_{k=-(N-1)}^{N-1}\chi_{\mathrm{s},k}(\tau-kT_{\mathrm{s}},f_{\mathrm{d}})\cdot\mathrm{e}^{\mathrm{j}\pi f_{\mathrm{d}}(N-1+k)T_{\mathrm{s}}}\frac{\sin\left[\pi f_{\mathrm{d}}(N-|k|)T_{\mathrm{s}}\right]}{\sin(\pi f_{\mathrm{d}}T_{\mathrm{s}})}. \tag{11}$$

3.1 Cause of time-delay dimension side peak

In order to analyze the time-delay dimension of ambiguity function, let $f_{\mathrm{d}}=0$ Hz in (11) and apply the limit

$$\lim_{f_{\mathrm{d}}\to0}\frac{\sin\left[\pi f_{\mathrm{d}}(N-|k|)T_{\mathrm{s}}\right]}{\sin(\pi f_{\mathrm{d}}T_{\mathrm{s}})}=\lim_{f_{\mathrm{d}}\to0}\frac{\pi(N-|k|)T_{\mathrm{s}}\cos\left[\pi f_{\mathrm{d}}(N-|k|)T_{\mathrm{s}}\right]}{\pi T_{\mathrm{s}}\cos(\pi f_{\mathrm{d}}T_{\mathrm{s}})}=N-|k|. \tag{12}$$

Then, we get

$$\chi(\tau,0)=\sum_{k=-(N-1)}^{N-1}(N-|k|)\chi_{s,k}(\tau-kT_s,0). \tag{13}$$

Because the information transmitted by each time slot is random, $\chi_{s,nm}$ in (7) has the following properties:

$$\chi_{s,00}\approx\chi_{s,11}\approx\cdots\approx\chi_{s,(N-1)(N-1)}\gg\chi_{s,nm}\approx 0\ ,\ n\neq m. \tag{14}$$

By applying the properties in (14), (13) can be simplified as

$$\chi(\tau,0)=N\chi_{s,0}(\tau,0). \tag{15}$$

It can be seen from (15) that the time-delay dimension of Link16 signal ambiguity function is equal to the superposition of autocorrelation of each time slot. $\chi_{s,0}(\tau,\ 0)$ is analyzed below.

Take the first time slot as an example. In (4), each pulse is down converted according to the following frequency hopping pattern:

$$\begin{aligned}u(t)=&\sum_{i=0}^{257}m_i(t-iT_p-T_j)\cdot\\ &e^{j2\pi(f_c+\Delta f_i)(t-iT_p-T_j)}e^{-j2\pi(f_c+\Delta f_i)(t-iT_p-T_j)}=\\ &\sum_{i=0}^{257}m_i(t-iT_p-T_j)\ ,\\ &iT_p+T_j\leqslant t\leqslant iT_p+T_{pd}+T_j.\end{aligned} \tag{16}$$

Substituting (16) into (5) and letting $f_d = 0$ Hz, we get

$$\begin{aligned}\chi_{s,0}(\tau,0)=&\int_{-\infty}^{+\infty}u(t)u^*(t-\tau)\,dt=\\ &\int_{-\infty}^{+\infty}\left(\sum_{i=0}^{257}m_i(t-iT_p-T_j)\right)\cdot\\ &\left(\sum_{l=0}^{257}m^*{}_l(t-lT_p-T_j-\tau)\right)dt=\\ &\sum_{i=0}^{257}\sum_{l=0}^{257}\int_{-\infty}^{+\infty}m_i(t-iT_p-T_j)m^*{}_l(t-lT_p-T_j-\tau)\,dt.\end{aligned} \tag{17}$$

Let $t'=t-iT_p-T_j$, then (17) can be written as

$$\begin{aligned}&\chi_{s,0}(\tau,0)=\\ &\sum_{i=0}^{257}\sum_{l=0}^{257}\int_{-\infty}^{+\infty}m_i(t')\,m^*{}_l(t'-[\tau-(i-l)T_p])\,dt'=\\ &\sum_{i=0}^{257}\sum_{l=0}^{257}\chi_{il}(\tau-(i-l)T_p,0)\end{aligned} \tag{18}$$

where the integral term in (18) represents the cross-correlation between the ith MSK modulated pulse and the lth MSK modulated pulse, expressed by χ_{il}. Because the pulse width is T_{pd}, the width of $\chi_{il}(\tau,\ 0)$ is approximately equal to $2T_{pd}$. And because $T_p > 2T_{pd}$, each χ_{il} does not overlap after T_p integral multiple translation in time domain. To sum up, it is a simple superposition of cross-correlation between single MSK modulated pulses after time-domain translation.

Because the baseband symbols modulated by MSK are random, and the same group of symbols in STDP package use two pulses for transmission, χ_{il} has the following approximate relationship:

$$\begin{aligned}&\chi_{00}\approx\chi_{11}\approx\chi_{22}\approx\cdots\approx\chi_{257\,257}\approx\\ &\chi_{01}\approx\chi_{23}\approx\chi_{45}\approx\cdots\approx\chi_{256\,257}\approx\\ &\chi_{10}\approx\chi_{32}\approx\chi_{54}\approx\cdots\approx\chi_{257\,256}\triangleq\\ &\chi_p\gg\chi_{il}\triangleq\chi_v\ ,\\ &\begin{cases}i\neq l\\ i\neq 2p+1,l\neq 2p,p=0,1,\cdots,128\\ i\neq 2p,l\neq 2p+1,p=0,1,\cdots,128\ .\end{cases}\end{aligned} \tag{19}$$

Let $i - l = n$, then for i, $l\in[0,257]$, there are 258 combinations that make $i-l = 0$, that is, $i=l$. There are $2\times(258-1)=514$ combinations that make $|i-l| = 1$, of which 258 combinations of i and l satisfy the condition that

$$\begin{cases}i=2p+1,l=2p\\ i=2p,l=2p+1\end{cases}$$

where $p=0,1,\cdots,128$.

By analogy, (18) can be rewritten as follows:

$$\begin{aligned}&\chi_{s,0}(\tau,0)=258\chi_p(\tau,0)+\\ &\sum_{2\leqslant|n|\leqslant257}[(258-|n|)\chi_v(\tau-nT_p,0)]+\\ &\sum_{|n|=1}[129\chi_p(\tau-nT_p,0)+128\chi_v(\tau-nT_p,0)].\end{aligned} \tag{20}$$

If only the part of $\tau \geqslant 0$ is considered, then (20) can be simplified as

$$\begin{aligned}&\chi_{s,0}(\tau,0)=258\chi_p(\tau,0)+\\ &[129\chi_p(\tau-T_p,0)+128\chi_v(\tau-T_p,0)]+\\ &\sum_{2\leqslant n\leqslant257}[(258-n)\chi_v(\tau-nT_p,0)].\end{aligned} \tag{21}$$

And the ambiguity function of MSK modulation signal [40] is

$$\chi_p(\tau,0)=\begin{cases}32\left(T_B-\dfrac{\tau}{2}\right)\cos\left(\dfrac{\pi\tau}{2T_B}\right)+\\ \qquad\dfrac{32T_B}{\pi}\sin\left(\dfrac{\pi\tau}{2T_B}\right),\ 0\leqslant\tau\leqslant2T_B\\ 0,\ 2T_B<\tau\leqslant31T_B\end{cases}. \tag{22}$$

It can be seen from (22) that $\chi_p(\tau, 0)$ has a peak value at $\tau = 0$. $\chi_v(\tau, 0)$ and $\chi_p(\tau, 0)$ have the same envelope, but the amplitude of $\chi_v(\tau, 0)$ is much lower than $\chi_p(\tau, 0)$. Therefore, the three terms in (21) satisfy

$$\begin{aligned} &258\chi_p(\tau,0) > \\ &[129\chi_p(\tau-T_p,0)+128\chi_v(\tau-T_p,0)] \gg \\ &[(258-n)\chi_v(\tau-nT_p,0)]. \end{aligned} \tag{23}$$

To sum up, in the zero Doppler cut, $\chi(\tau, 0)$ has a peak at $\tau = 0$, and side peaks appear at $\tau = nT_p$ ($n = 1, 2, \cdots$) with T_p as the period. The position where the first side peak appears is $\tau = T_p$, and its amplitude is the largest compared with other side peaks.

3.2 Cause of Doppler dimension side peak

In order to analyze the Doppler dimension of ambiguity function, let $\tau = 0$ in (11) and we can get

$$\begin{aligned} \chi(0,f_d) = &\mathrm{e}^{\mathrm{j}2\pi f_d T_j}\sum_{k=-(N-1)}^{N-1}\chi_{s,k}(-kT_s,f_d)\cdot \\ &\mathrm{e}^{\mathrm{j}\pi f_d(N-1+k)T_s}\frac{\sin[\pi f_d(N-|k|)T_s]}{\sin(\pi f_d T_s)}. \end{aligned} \tag{24}$$

Ignore the phase term in (24) and applying the properties in (14), (24) can be simplified to

$$\chi(0,f_d) = \chi_{s,0}(0,f_d)\frac{\sin(\pi f_d N T_s)}{\sin(\pi f_d T_s)}. \tag{25}$$

In (25), the term $\sin(\pi f_d N T_s)/\sin(\pi f_d T_s)$ has a peak value at $f_d = n / T_s$ (n is an integer), and it has the zero point at $f_d = k / (NT_s)$ (k is a non-zero integer). It can be seen that the Doppler dimensional envelope of Link16 signal ambiguity function is equal to $\chi_{s,0}(0, f_d)$, and the interior is filled with $\sin(\pi f_d N T_s)/\sin(\pi f_d T_s)$. Next, $\chi_{s,0}(0, f_d)$ is analyzed.

As in the previous section, taking the first time slot as an example, set $N = 1$ in (4), then substitute (16) into (5), and set $\tau = 0$, we can get

$$\begin{aligned} &\chi_{s,0}(0,f_d) = \int_{-\infty}^{+\infty}u(t)u^*(t)\mathrm{e}^{\mathrm{j}2\pi f_d t}\mathrm{d}t = \\ &\int_{-\infty}^{+\infty}\left(\sum_{i=0}^{257}m_i(t-iT_p-T_j)\right)\cdot\left(\sum_{l=0}^{257}m^*{}_l(t-lT_p-T_j)\right)\mathrm{e}^{\mathrm{j}2\pi f_d t}\mathrm{d}t = \\ &\sum_{i=0}^{257}\sum_{l=0}^{257}\int_{-\infty}^{+\infty}m_i(t-iT_p-T_j)m^*{}_l(t-lT_p-T_j)\mathrm{e}^{\mathrm{j}2\pi f_d t}\mathrm{d}t. \end{aligned} \tag{26}$$

Similar to the above analysis method, (26) can be further written as

$$\begin{aligned} &\chi_{s,0}(0,f_d) = \\ &\sum_{k=-257}^{257}\chi_k(-kT_p,f_d)\frac{\sin[\pi f_d(258-|k|)T_p]}{\sin(\pi f_d T_p)} \approx \\ &\chi_0(0,f_d)\frac{\sin(258\pi f_d T_p)}{\sin(\pi f_d T_p)} = \\ &32T_B\,\mathrm{sinc}(32T_B\pi f_d)\frac{\sin(258\pi f_d T_p)}{\sin(\pi f_d T_p)}. \end{aligned} \tag{27}$$

In (27), the term $\mathrm{sinc}(32T_B\pi f_d)$ takes the peak value at $f_d = 0$ Hz, and it takes the first zero point at $f_d = \pm 1/(32T_B) = \pm 156\,250$ Hz. And in the range of Doppler frequency shift $-2\,000$ Hz $\leqslant f_d \leqslant 2\,000$ Hz, the term $\mathrm{sinc}(32T_B\pi f_d) \approx 1$, thus

$$\chi_{s,0}(0,f_d) \approx 32T_B\frac{\sin(258\pi f_d T_p)}{\sin(\pi f_d T_p)}. \tag{28}$$

It can be seen from (28) that $\chi_{s,0}(0, f_d)$ takes the peak value at $f_d = 0$ Hz, and takes the zero point at $f_d = k/(258T_p)$, k is the non-zero integer. Fig. 9 shows the curve in Fig. 8(c) where the zero range cut is normalized but without decibels, the dashed line is the envelope of $\sin(\pi f_d N T_s)/\sin(\pi f_d T_s)$, and its analytic formula is $\sin(258\pi f_d T_p)/\sin(\pi f_d T_p)$. The first side peak of $\chi(0, f_d)$ is located at $f_d = \pm 1/T_s = \pm 128$ Hz, which has the largest amplitude compared with other side peaks. The zero point is located at $f_d = \pm 298$ Hz, ± 596 Hz, ± 894 Hz, and $\pm 1\,193$ Hz, which is also the reason for the formation of several zero lines in Fig. 8(c).

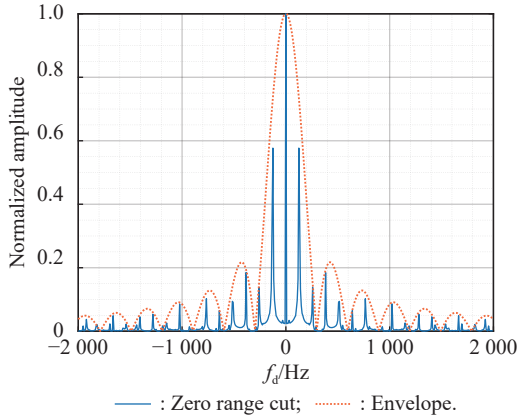

Fig. 9 Zero range cut of ambiguity function

4. Side peaks suppression method

From the analysis and simulation results in Section 3, it can be seen that there are many side peaks with high amplitude in the ambiguity function of Link16 signal, which will lead to the appearance of false targets in tar-

get detection, so it is necessary to suppress the side peaks. On the basis of Section 3, this section will propose a method to suppress side peak of Link16 signal.

It can be seen from the analysis in Subsection 3.1 that the periodic pulse structure of Link16 signal in time domain causes side peaks with high amplitude in time-delay dimension. In analog television (ATV) based passive radar, Wang et al. [11] used the MMF algorithm in binary phase-coded radar to suppress the time-delay dimension side peaks caused by the periodicity of 64 μs continuous line signal which transmits ATV picture. However, the Link16 signal used in this paper is a discrete signal truncated by pulse in time domain, and the two adjacent time slots have strong correlation. The cost function in [11] only restricts the energy at the side peak, and cannot effectively suppress the side peak of Link16 signal. Therefore, in this paper, the improved NMMF algorithm is proposed to suppress the side peaks.

NMMF suppresses the energy in the side peak and its neighborhood by constructing a cost function and controls the output signal-to-noise ratio loss caused by mismatch. The cost function can be written as

$$\min_{\boldsymbol{w}_{\text{mis}}} J = [\boldsymbol{w}_{\text{mis}} - \boldsymbol{w}]^{\text{H}} [\boldsymbol{w}_{\text{mis}} - \boldsymbol{w}] + \sum_{d} \sum_{k \in U(d,\delta)} c_d \boldsymbol{w}_{\text{mis}}{}^{\text{H}} \boldsymbol{s}(k) \boldsymbol{s}^{\text{H}}(k) \boldsymbol{w}_{\text{mis}} \tag{29}$$

where $\boldsymbol{w}_{\text{mis}} \in \mathbf{C}^{L\times 1}$ is the NMMF factor to be solved; $\boldsymbol{w} = [s(0), s(1), \cdots, s(l-1)]^{\text{T}}$ is the MF factor; c_d is a weighted factor and $c_d > 0$; d is the position of time-delay dimension side peak; $U(d, \delta)$ is the δ neighborhood of point d, and $U(d, \delta) = \{k \in \mathbf{Z} |\ d-\delta \leqslant k \leqslant d+\delta\}$; $\boldsymbol{s}(k) = [s(k), s(k+1), \cdots, s(k+L-1)]^{\text{T}}$, and L is the length of Link16 signal.

The Hessian matrix of the cost function J is

$$\boldsymbol{E} = \nabla^2 J = 2\left(\boldsymbol{I}_L + \sum_{d} \sum_{k \in U(d,\delta)} c_d \boldsymbol{s}(k) \boldsymbol{s}^{\text{H}}(k)\right) \geqslant 0 \tag{30}$$

where $\boldsymbol{I}_L$ is an $L\times L$ identity matrix. It can be seen that $\boldsymbol{E}$ is a positive semi-definite matrix when $c_d > 0$. From the second-order necessary and sufficient condition of convex function, we know J is a convex function. When $\nabla J = 0$, the NMMF factor obtains the optimal solution, where

$$\nabla J = \frac{\partial J}{\partial \boldsymbol{w}_{\text{mis}}{}^{\text{H}}} = 2\left(\boldsymbol{w}_{\text{mis}} - \boldsymbol{w} + \sum_{d} \sum_{k \in U(d,\delta)} c_d \boldsymbol{s}(k) \boldsymbol{s}^{\text{H}}(k) \boldsymbol{w}_{\text{mis}}\right). \tag{31}$$

Therefore, the optimal solution of the NMMF factor is

$$\boldsymbol{w}_{\text{mis}} = \left[\boldsymbol{I}_N + \sum_{d} \sum_{k \in U(d,\delta)} c_d \boldsymbol{s}(k) \boldsymbol{s}^{\text{H}}(k)\right]^{-1} \boldsymbol{w}. \tag{32}$$

In order to obtain higher integration gain, the passive radar often has a longer coherent integration time, which makes the signal length L very large (tens of thousands or more). It can be seen from (32) that the inverse of L-order matrix is required when calculating the NMMF factor, and corresponding to $O[(2\delta + 1)dL^2 + L^2 \log_2 L]$ complex products. This will cost huge computing resources, and it is difficult to achieve. In order to reduce the computation burden, the batch version of the NMMF algorithm is proposed next.

The batch version algorithm divides the NMMF factor into B segments, each segment's length is L_B, and satisfies $L=BL_B$, which can be expressed as $\boldsymbol{w}_{\text{mis}} = \left[(\boldsymbol{w}_{\text{mis}}^0)^{\text{T}}, (\boldsymbol{w}_{\text{mis}}^1)^{\text{T}}, \cdots, (\boldsymbol{w}_{\text{mis}}^{B-1})^{\text{T}}\right]^{\text{T}}$. And the optimal solution of each segment NMMF factor is

$$\boldsymbol{w}_{\text{mis}}^b = \left(\boldsymbol{I}_{L_B} + \sum_{d} \sum_{k \in U(d,\delta)} c_d \boldsymbol{s}_b(k) \boldsymbol{s}_b{}^{\text{H}}(k)\right)^{-1} \boldsymbol{w}_b \tag{33}$$

where $\boldsymbol{w}_{\text{mis}}^b \in \mathbf{C}^{L_B\times 1} (b = 0, 1, \cdots, B-1)$ is the segmented NMMF factor; $\boldsymbol{I}_{L_B}$ is an $L_B \times L_B$ identity matrix, and $\boldsymbol{s}_b(k) = [s(k + bL_B), s(k + 1 + bL_B), \cdots, s(k + L_B - 1 + bL_B)]^{\text{T}}$, $\boldsymbol{w}_{\text{b}} = [s(bL_B), s(1 + bL_B), \cdots, s(L_B - 1 + bL_B)]^{\text{T}}$. The evaluation of each batch's NMMF factor $\boldsymbol{w}_{\text{mis}}^b$ corresponds to only $O[(2\delta + 1)dL_B{}^2 + L_B{}^2 \log_2 L_B]$ complex products. It can be clearly seen that the evaluation of all batches are $O[(2\delta + 1)dL_BL + L_BL \log_2 L_B]$ complex products. It is obvious that the batch version can acquire great computational saving compared to the original one as long as $L_B \ll L$.

According to the analysis of Subsection 3.1, let $d = mT_{\text{p}}f_{\text{s}}$ (m = 1, 2, ⋯, 15) in (33), and the simulation results are shown in Fig. 10. The blue solid line shows the zero Doppler cut after suppressing the side peaks using NMMF algorithm, the green dotted line is the result of using the MMF algorithm in [11], and the red dashed line is the result of MF. It can be clearly seen that when the NMMF algorithm is used to suppress the side peaks, the amplitude of the first side peak decreases by 13.69 dB, while the amplitudes of the other side peaks are below −25 dB. The result of the MMF algorithm in [11] is similar to MF, which cannot effectively suppress the time-delay dimension side peaks.

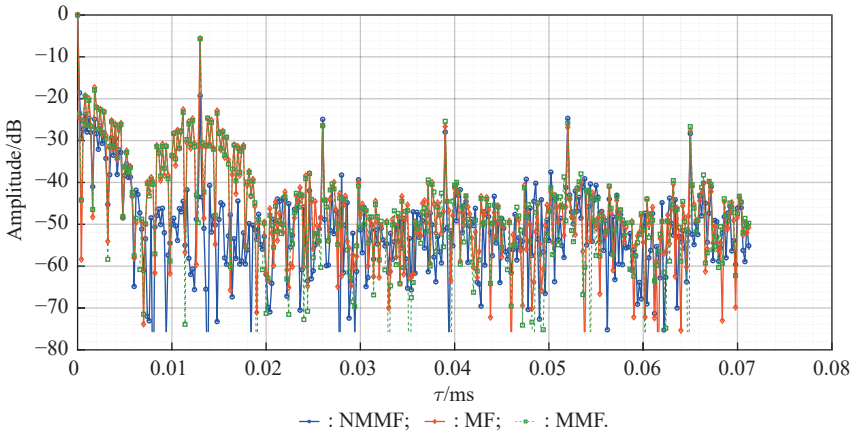

Fig. 10 Zero Doppler cut result of NMMF

From the analysis of Subsection 3.2, it is known that the Doppler side peaks are caused by the pulse structure of the time slot. In order to suppress the Doppler side peak, the jitter and propagation corresponding to the NMMF factor and Link16 signal need to be removed, and then the remaining effective parts of the time slot need to be spliced together. After the above processing, the Doppler dimension side peaks can be eliminated. The result is shown in Fig. 11.

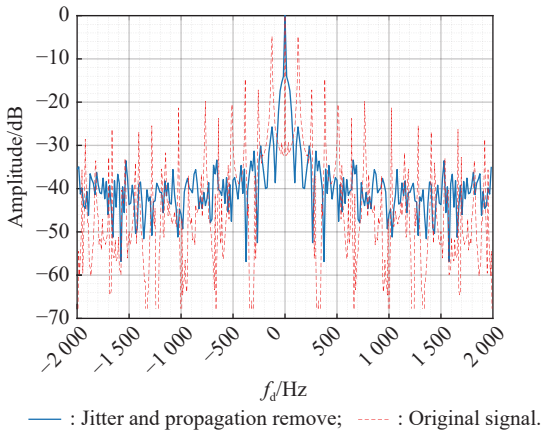

Fig. 11 Zero range cut after removing jitter and propagation

Compared with the unremoved original signal, the amplitude of the first side peak in Doppler dimension has decreased by 20.95 dB, and the side peaks in the other positions are below −25.73 dB.

To sum up, the side peaks suppression method of Link16 signal ambiguity function is shown in Fig. 12, and the ambiguity function after side peaks suppression is shown in Fig. 13.

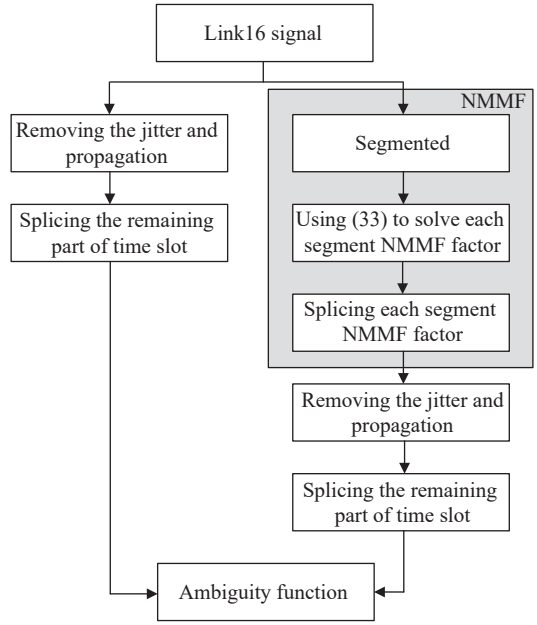

Fig. 12 Flowchart of side peaks suppression method

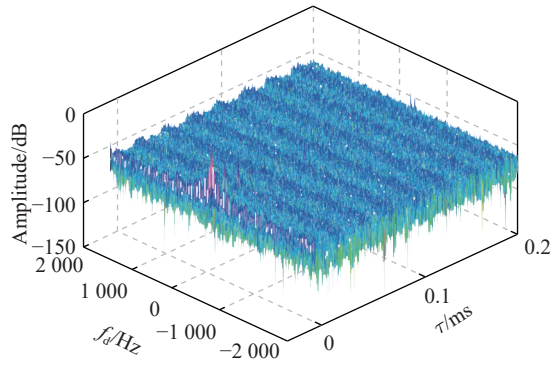

Fig. 13 Ambiguity function after side peaks suppression

5. Conclusions

This paper discusses the possibility of using Link16 signal as the opportunity illuminator of passive radar to

detect targets. Firstly, the structure of Link16 signal is analyzed in detail, and the time domain expression of Link16 signal is given. Then, the ambiguity function expression of Link16 signal is deduced, and the causes of time-delay and Doppler dimension side peaks are analyzed with the simulation results. Subsequently, according to the causes of the side peaks, the methods of suppressing time-delay and Doppler dimension side peak are proposed, in which the NMMF algorithm is proposed when suppressing the time-delay dimension side peaks. The experimental results show that the proposed algorithm can effectively suppress the side peaks, which provides a theoretical basis for Link16 based passive radar.

References

[1] HOWLAND P E, MAKSIMIUK D, REITSMA G. FM radio based bistatic radar. IEE Proceedings-Radar, Sonar and Navigation, 2005, 152(3): 107–115.

[2] WANG J, BAO Z, ZHANG S H. Passive detecting/tracking radar system technologies and its development. Radar Science and Technology, 2004(3): 129–135. (in Chinese)

[3] LAURI A, COLONE F, CARDINALI R, et al. Analysis and emulation of FM radio signals for passive radar. Proc. of the IEEE Aerospace Conference, 2007. DOI: 10.1109/AERO.2007.353068.

[4] MALANOWSKI M, KULPA K, KULPA J, et al. Analysis of detection range of FM-based passive radar. IET Radar, Sonar & Navigation, 2014, 8(2): 153–159.

[5] SHI C G, ZHOU J J, WANG F. Cramer Rao bound analysis for joint target location and velocity estimation in FM-based passive radar networks. IET Signal Processing, 2016, 10(7): 780−790.

[6] CHOI S, CROUSE D F, WILLETT P, et al. Approaches to Cartesian data association passive radar tracking in a DAB/DVB network. IEEE Trans. on Aerospace and Electronic Systems, 2014, 50(1): 649–663.

[7] COLEMAN C J, WATSON R A, YARDLEY H. A practical bistatic passive radar system for use with DAB and DRM illuminators, Proc. of the IEEE Radar Conference, 2008. DOI: 10.1109/RADAR.2008.4721007.

[8] COLEMAN C, YARDLEY H. Passive bistatic radar based on target illuminations by digital audio broadcasting. IET Radar, Sonar & Navigation, 2008, 2(5): 366–375.

[9] HOWLAND P E. A passive metric radar using a transmitter of opportunity. Proc. of the International Conference of Radar, 1994: 370−375.

[10] HOWLAND P F. Target tracking using television-based bistatic radar. IEE Proceedings-Radar, Sonar and Navigation, 1999, 146(3): 166–174.

[11] WANG H, WANG J, ZHONG L. Mismatched filter for analogue TV-based passive bistatic radar. IET Radar, Sonar & Navigation, 2011, 5(5): 573–581.

[12] SAINI R, CHERNIAKOV M. DTV signal ambiguity function analysis for radar application. IEE Proceedings-Radar, Sonar and Navigation, 2005, 152(3): 133–142.

[13] GAO Z W, TAO R, SHAN T, Side peaks analysis and suppression of DVB-T signal ambiguity function for passive radar. Acta Electronic Sinica, 2008, 36(3): 505−509.

[14] ZUO L, WANG J, ZHAO T, et al. A joint low-rank and sparse method for reference signal purification in DTMB-based passive bistatic radar. Sensors, 2021, 21(11): 3607.

[15] PALMER J E, HARMS H A, SEARLE S J, et al. DVB-T passive radar signal processing. IEEE Trans. on Signal Processing, 2013, 61(8): 2116–2126.

[16] SOLODKY G, LONGMAN O, VILLEVAL S, et al. CDMA-MIMO radar with the TANSEC waveform. IEEE Trans. on Aerospace and Electronic Systems, 2020, 57(1): 76–89.

[17] BOURNAKA G, UMMENHOFER M, CRISTALLINI D, et al. Experimental study for transmitter imperfections in DVB-T based passive radar. IEEE Trans. on Aerospace and Electronic Systems, 2017, 54(3): 1341–1354.

[18] FANG Y, ATKINSON G, SAYIN A, et al. Improved passive SAR imaging with DVB-T transmissions. IEEE Trans. on Geoscience and Remote Sensing, 2020, 58(7): 5066–5076.

[19] TAN D K P, SUN H, LU Y, et al. Passive radar using global system for mobile communication signal: theory, implementation and measurements. IEE Proceedings-Radar, Sonar and Navigation, 2005, 152(3): 116–123.

[20] WANG H T, WANG J, LI H W. Target detection using CDMA based passive bistatic radar. Journal of Systems Engineering and Electronics, 2012, 23(6): 858–865.

[21] RAJA R A, NOOR A A, NUR A R, et al. Analysis on target detection and classification in LTE based passive forward scattering radar. Sensors, 2016, 16(10): 1607.

[22] WAN X R, LIU T T, YI J X, et al. System design and target detection experiments for LTE-based passive radar. Journal of Radars, 2020, 9(6): 967–973. (in Chinese)

[23] LU X D, ZHANG H L, LIU Z S, et al. Research on co-channel base station interference suppression method of passive radar based on LTE signal. Journal of Electronics & Information Technology, 2019, 41(9): 2123–2130.

[24] MEI W H, CAI S F. JTIDS/Link 16 data link. Beijing: National Defense Industry Press, 2007. (in Chinese)

[25] CHEN G. Study on target detection and interference suppression for passive bistatic radar. Xi'an: Xidian University, 2020.

[26] GUO H, COETZEE S, MASON D, et al. Passive radar detection using wireless networks. Heart, 2007. DOI: 10.1049/cp:20070643.

[27] COLONE F, WOODBRIDGE K, GUO H, et al. Ambiguity function analysis of wireless LAN transmissions for passive radar. IEEE Trans. on Aerospace and Electronic Systems, 2011, 47(1): 240–264.

[28] RAO Y H, ZHU F Y, ZHANG X Z, et al. Ambiguity function analysis and side peaks suppression of WiFi signal for passive radar. Journal of Radars, 2012, 1(3): 225–231.

[29] COLONE F, FALCONE P, BONGIOANNI C, et al. WiFi-based passive bistatic radar: data processing schemes and experimental results. IEEE Trans. on Aerospace and Electronic Systems, 2012, 48(2): 1061–1079.

[30] WAN X R, CEN B, CHENG F, et al. Ambiguity function analysis and processing of CMMB signal based passive radar. Journal of Electronics and Information Technology, 2011, 33(10): 2489–2493.

[31] WANG T Y, LIU B, WANG X L , et al. Passive radar analysis using DTMB signal. Proc. of the 19th International Conference on Optical Communications and Networks, 2021. DOI: 10.1109/ICOCN53177.2021.9563834.

[32] TAO R, GAO Z W, WANG Y. Side peaks interference suppression in DVB-T based passive radar. IEEE Trans. on Aerospace and Electronic Systems, 2012, 48(4): 3610–3619.

[33] RICHARDS MARK A. Fundamentals of radar signal pro-

cessing. New York: McGraw-Hill Education, 2014.
[34] CHEN G, WANG J, GUO S, et al. Improved mismatched filtering for ATV-based passive bistatic radar. IET Radar, Sonar & Navigation, 2018, 12(6): 663–670.
[35] CHEN G, WANG J. Robust mismatched filtering algorithm for passive bistatic radar using worst-case performance optimization. Frontiers of Information Technology & Electronic Engineering, 2020, 21(7): 1074–1084.
[36] WANG Z F, LIAO G S, YANG Z W. Space-frequency modulation radar-communication and mismatched filtering. IEEE Access, 2018, 6: 24837–24845.
[37] FAN C X, CAO L N. Priciples of communications. 6th edition. Beijing: National Defense Industry Press, 2010. (in Chinese)
[38] CHEN B X. Mordern radar system analysis and design. Xi'an: Xidian University Press, 2012.
[39] RIHACZEK A W. Principles of high-resolution radar. Norwood, MA: Artech House, 1996.
[40] ZHAO X H, RAN T, YUE W. Analytical expression of GSM signal ambiguity function. Proc. of the International Conference on Signal Processing, 2008. DOI: 10.1109/ICOSP.2008.4697604.

Biographies

BAI Luyang was born in 1997. He received his B.S. degree in the School of Information and Control Engineering in 2019 from China University of Mining and Technology, Xuzhou, China. He is pursuing his M.S. degree in National Laboratory of Radar Signal Processing from Xidian University, Xi'an, China. His research interests include passive radar signal processing and passive multiple input and multiple output radar.
E-mail: lybai_19@stu.xidian.edu.cn

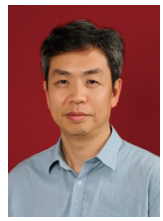

WANG Jun was born in 1969. He received his B.S. degree in measurement engineering, M.S. and Ph.D. degrees in signal and information processing from Xidian University in 1990, 1995, and 2000, respectively. He joined the National Laboratory of Radar Signal Processing in Xidian University in 1995, where he served as a lecturer from 1996 to 2000, and an associated professor from 2000 to 2004. Since 2004, he has been a professor in the National Laboratory of Radar Signal Processing. He is also a senior member of Chinese Institute of Electronics. He serves as a reviewer for the IET Radar, Sonar & Navigation and Electronics Letters, Journal of Systems Engineering and Electronics. His current research interests include passive coherent detection and location, radar imaging, and weak signal detection.
E-mail: wangjun@xidian.edu.cn

CHEN Xiaoling was born in 1997. She received her B.S. degree in electronic and information engineering from Xidian University in 2019. She is pursuing her M.S. degree in National Laboratory of Radar Signal Processing from Xidian University, Xi'an, China. Her research interests include terahertz multiple input and multiple output array signal processing and imaging method.
E-mail: cxl120100@163.com